Palaeogeography, Palaeoclimatology, Palaeoecology 701 (2026) 114173

Contents lists available at ScienceDirect

Palaeogeography, Palaeoclimatology, Palaeoecology

journal homepage: www.elsevier.com/locate/palaeo

Latitudinal controls on carbonate factory evolution following the Carnian Pluvial Episode: Insights from the Tibetan Himalaya

Tianhao Su [a], Zhong Han [b,*], Yixing Du [c], Jingxin Jiang [a], Xiumian Hu [a]

[a] State Key Laboratory of Critical Earth Material Cycling and Mineral Deposits, School of Earth Sciences and Engineering, Nanjing University, Nanjing 210023, China
[b] State Key Laboratory of Palaeobiology and Stratigraphy, Nanjing Institute of Geology and Palaeontology, Chinese Academy of Sciences, Nanjing 210008, China
[c] State Key Laboratory of Oil and Gas Reservoir Geology and Exploitation, Institute of Sedimentary Geology, Chengdu University of Technology, Chengdu 610059, China

A R T I C L E I N F O

Editor: S Shen

Keywords:
CPE
Carbonate factory
Tibetan Himalaya
Microfacies analysis
Latitudinal control
Late Triassic

A B S T R A C T

The Carnian Pluvial Episode (CPE) is characterized by multiple negative carbon isotope excursions driven by massive CO_2 emissions from the Wrangellia Large Igneous Province. Intense environmental perturbations during the CPE reorganized low-latitude carbonate factories. In paleo-tropic regions (e.g., Italy, Sichuan Basin), this triggered a shift to metazoan-dominated factories, followed by a post-CPE resurgence of microbial factories. However, the global relevance of this pattern remains uncertain. Here, we present a high-resolution microfacies and conodont biostratigraphy dataset from the subtropical Tibetan Himalaya to reconstruct Late Carnian–Early Norian carbonate platform evolution. Our results show the upper Qulonggongba Formation (Tuvalian 2) was deposited in a terrigenous-influenced mixed inner ramp, while the overlying Qimala Formation (Tuvalian 2–Lacian) developed in a middle-to-outer ramp environment. After the CPE, the western Tibetan Himalaya carbonate factory shifted from a metazoan-dominated skeletal factory to a productive peloidal factory. Crucially, petrographic evidence indicates these peloids predominantly originated from micritized bioclasts and reworked carbonate mud, demonstrating the system remained fundamentally driven by heterotrophic metazoans rather than transitioning to a microbial factory. This post-CPE heterogeneity among Tethyan domains is largely due to latitudinal controls on surface seawater temperature and carbonate saturation. Additionally, paleogeographic configurations further differentiated recovery patterns: semi-restricted, tropical low-latitudes favored microbial factories, whereas the subtropical, open-marine conditions of the Tibetan Himalaya sustained heterotrophic metazoan dominance.

1. Introduction

The Carnian Pluvial Episode (CPE) represents a profound environmental perturbation during the Late Triassic, marked by a dramatic intensification of the global hydrological cycle and a pulsed influx of terrigenous materials in the late Early Carnian (Julian 2). This environmental perturbation triggered a crisis in shallow-marine carbonate production, lithologically evidenced by the widespread replacement of carbonate sediments with siliciclastic deposits (Keim et al., 2006; Hornung et al., 2007a, 2007b; Rigo et al., 2007; Lukeneder et al., 2012; Preto et al., 2013; Gattolin et al., 2015; Sun et al., 2016). Carbon isotope stratigraphy from both marine and terrestrial sections reveals that the onset of the CPE (Julian 1–Julian 2 boundary, ~234 Ma) coincided with an abrupt negative carbon isotope excursion (NCIE) as well as an intensified hydrological cycle, accompanied by repeated isotopic fluctuations (Dal Corso et al., 2012, 2015, 2018; Mueller et al., 2016; Sun et al., 2016; Miller et al., 2017; Fu et al., 2020; Lu et al., 2021; Ke et al., 2023; Jia et al., 2025). These NCIEs coupled with the hydrological cycle amplification, are widely interpreted as the results of global warming driven by CO_2 emissions from the multiphase emplacement of the Wrangellia Large Igneous Province (LIP) (Furin et al., 2006; Greene et al., 2010; Dal Corso et al., 2012, 2015, 2020; Sun et al., 2016; Hu et al., 2020; Pecorari et al., 2023).

Geochronological data from the Wrangellia igneous rocks of Vancouver Island (Canada) and Alaska (USA), combined with the ammonite constraints, constrain the termination of LIP activity to the end of the Tuvalian 1 substage (~233 Ma; Mortensen and Hulbert, 1991; Tozer, 1994; Greene et al., 2010). Following the cessation of volcanic activity, shallow-marine carbonate deposition—previously disrupted by the CPE—recovered in Early Tuvalian 2 (De Zanche et al., 2000; Preto and

* Corresponding author.
E-mail address: zhonghan@nigpas.ac.cn (Z. Han).

https://doi.org/10.1016/j.palaeo.2026.114173
Received 25 February 2026; Received in revised form 16 August 2026; Accepted 22 August 2026
Available online 24 August 2026

Hinnov, 2003; Hornung et al., 2007b; Roghi et al., 2010; Lukeneder et al., 2012; Sun et al., 2016; Dal Corso et al., 2018). During the CPE, enhanced terrigenous input not only suppressed carbonate accumulation but also drove a major reorganization of carbonate producers. Evidence from the Dolomites (Italy) indicates that carbonate factories transitioned from microbial-dominated systems to those dominated by metazoan skeletons (e.g., bivalves, echinoderms, and brachiopods; Dal Corso et al., 2015, 2018). Subsequently, the post-CPE interval (Tuvalian 2) witnessed the resurgence of microbial carbonate factories (Caggiati et al., 2018). A parallel trajectory of carbonate factory evolution has been documented in the Sichuan Basin (Jin et al., 2018, 2019, 2020).

Skeletal metazoans rose to prominence in the Early Paleozoic and gradually dominated Phanerozoic shallow-marine carbonate deposition by establishing either tropical or cool-water factories. Since then, microbial carbonate factories have been more prone to develop during episodes of mass extinction events and carbonate production crises (Schlager, 2003; Riding and Liang, 2005). However, sedimentary records from Italy and the Sichuan Basin indicate an anomalous evolutionary pattern: metazoan skeletal factories dominated during the carbonate crisis of the CPE, whereas microbial factories prevailed after the CPE. Determining whether this phenomenon is global requires independent verification from regions geographically distinct from these well-studied areas. This study provides a new high-resolution stratigraphic and sedimentological investigation in the Tibetan Himalaya (southern Tibet) and aims to: (1) reconstruct the post-CPE evolutionary trajectory of carbonate factories in this region; and (2) investigate the global spatiotemporal patterns of carbonate factories and their controlling factors through regional and global correlation.

2. Geological background

2.1. Tectonic setting

The Tethyan Himalaya represents a stable passive continental margin from the Triassic to the end of the Cretaceous, with a continuous succession of marine sedimentary rocks (Garzanti, 1999; Sciunnach and Garzanti, 2012). Paleomagnetic reconstructions indicate that the Tethyan Himalaya was located in the Southern Hemisphere during the Late Triassic, corresponding to paleolatitudes ranging from approximately 25°S to 35°S (e.g., Klootwijk and Bingham, 1980; Appel et al., 1991; Ran et al., 2012; Fig. 1A). The studied Jiesheng Section is situated in Zanda County (the western Tibetan Himalaya) (Fig. 1B), and it is adjacent to the Spiti, from which previous researchers have recovered the Carnian Pluvial Episode succession (Hornung et al., 2007b).

2.2. Stratigraphy

The Jiesheng Section exposes a continuous Upper Triassic sequence comprising the upper Qulonggongba and Qimala formations. The upper Qulonggongba Formation (~117 m thick) represents a mixed

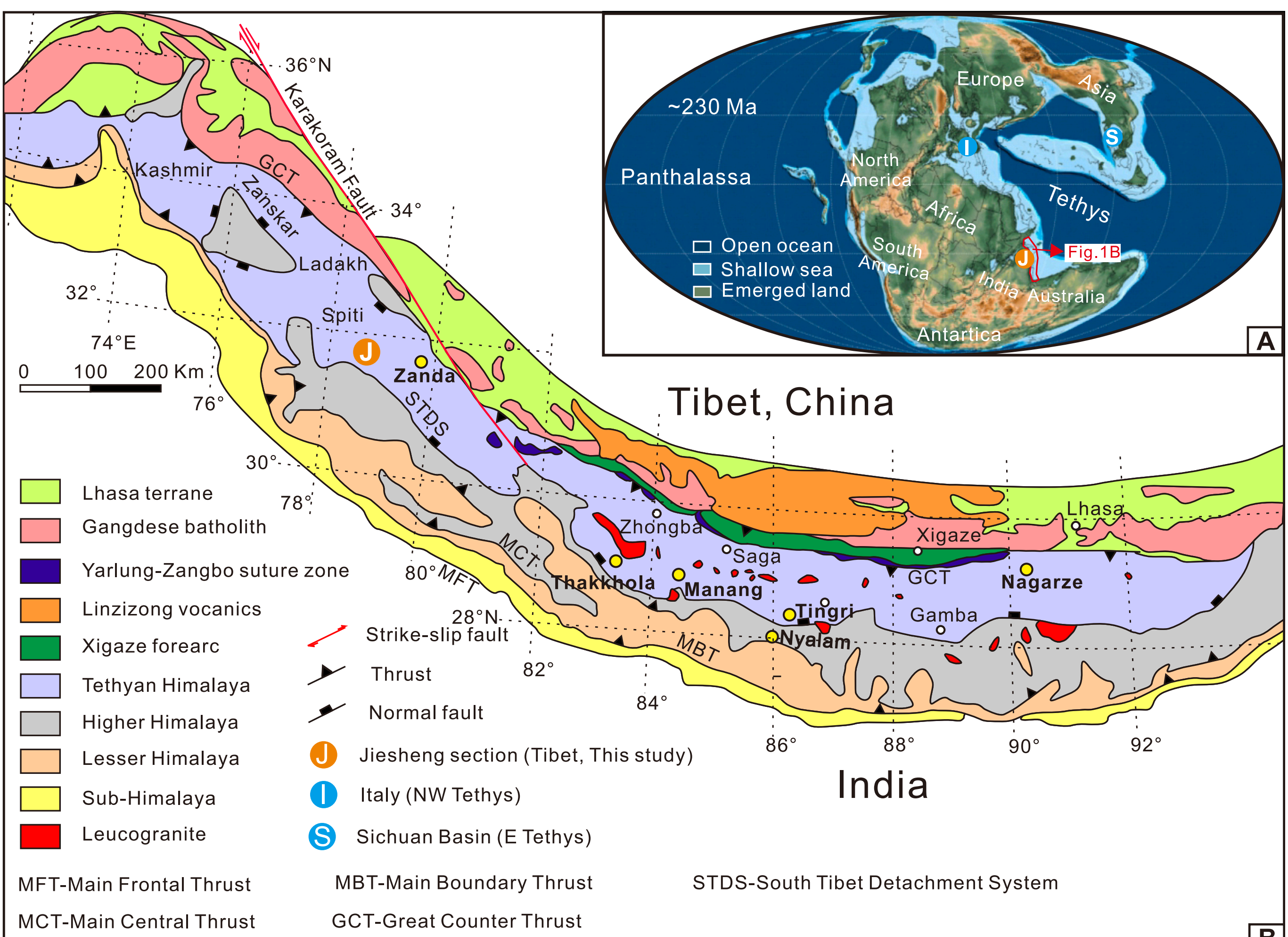

Fig. 1. (A) Paleogeographic map of the Late Triassic (~230 Ma) (modified after Scotese and Schettino, 2017). The red line indicates the location of the Tethys Himalaya. (B) Geological map of Himalaya (modified after Hu et al., 2016). (For interpretation of the references to colour in this figure legend, the reader is referred to the web version of this article.)

siliciclastic–carbonate succession, predominantly composed of yellow sandy limestone interbedded with micritic and bioclastic limestone (Du et al., 2024). Although earlier biostratigraphic studies based on bivalves and ammonoids found in basal horizons broadly assigned the whole Qulonggongba Formation to the Carnian–Norian interval (Zhang et al., 2015), recent high-resolution conodont analysis (e.g., *Paragondolella noah*, *P. oertlii*, *Metapolygnathus* cf. *mersinensis*, *M.* cf. *linguiformis*, *Carnepigondolella* cf. *zoae*, *C. tuvalica*, *M. praecommunisti*) constrains the studied upper Qulonggongba Formation to a Middle Tuvalian age (Du et al., 2024).

Conformably overlying this unit is the Qimala Formation, which consists primarily of micritic limestone, bioclastic, and peloidal limestone, with sandy limestone restricted to the basal intervals (Du et al., 2024). On the base of bivalve and ammonoid biostratigraphy, the unit was constrained to the Norian (Zhang et al., 2015). However, this is further refined by conodont assemblages (e.g., *Ancyrogondolella quadrata*), which date the Qimala Formation to the Late Carnian–Early Norian (Du et al., 2024).

3. Materials and methods

A total of 245 samples were systematically collected from the Jiesheng Section at a sampling interval of 1–2 m. To further refine the stratigraphic framework established by Du et al. (2024), we collected six additional conodont samples and one in-situ coral specimen. The conodont-bearing rock samples were crushed and treated with 8% acetic acid. The residual material was then washed, sieved through a 100 μm mesh sieve, and dried in a constant-temperature oven at 40 °C. Specimen identification of the conodonts was carried out at Chengdu University of Technology. For the coral sample, transverse thin sections were prepared to examine skeletal structure for taxonomic identification.

Carbonate microfacies analysis was conducted on 245 thin sections to determine grain types and content, fossil assemblages, and sedimentary textures. Carbonate rocks with <10% terrigenous material were classified according to Dunham (1962) and Embry and Klovan (1971), whereas mixed siliciclastic–carbonate sediments (>10% terrigenous material) were named following Mount (1985). Notably, in such classification schemes, the term mudstone refers to micritic limestone, rather than to clay-dominated mudrock in siliciclastic rock systems. Quantitative grain-composition analysis was conducted using the point-counting method, with analyses carried out in the JMicroVision software (https://jmicrovision.github.io/) and 300 points per sample were counted. Three main component groups were quantified: terrigenous grains (quartz, feldspar, and mica), skeletal grains (bivalves, ostracods, echinoderms, foraminifera, etc.), and non-skeletal grains (predominantly peloids). The evolution of carbonate factories was reconstructed using a "process–product" approach (Pomar and Hallock, 2008; Brandano et al., 2022).

4. Conodont biostratigraphy

The biostratigraphic framework of the Jiesheng Section has been recently established by Du et al. (2024), who subdivided the succession into three intervals: (1) the interval from the base to ~206 m is assigned to the Middle–Late Tuvalian (Late Carnian); (2) the interval from ~206 m to ~239 m represents the transition across the Carnian–Norian boundary; and (3) the strata above ~239 m are correlated to the Lacian (Early Norian). Conodonts in this study were successfully identified in three samples (JS204, JS214 and JS244; Fig. 2) and coral in JS221.

Our new paleontological data align well with and further corroborate this zonation (Fig. 3). The first occurrence of the conodont *Primatella triangulare* near sample JS106 marks the boundary between the Tuvalian 2 and Tuvalian 3 substages. Furthermore, the recovery of *Carnepigondolella pseudoechinata* (Fig. 2 1a-c) from sample JS204 falls within the proposed Carnian–Norian transitional interval (~206 m to ~239 m). This species typically ranges from the Late Tuvalian (Carnian) to Early Lacian (Norian) in the Tethyan realm (Mazza et al., 2012), thereby supporting the transitional age assignment. The conodont assemblage above JS212 consists of Lacian taxa, which is consistent with the stratigraphic data by Du et al. (2024) (Fig. 3). Additionally, the presence of the scleractinian coral *Retiophyllia* type IV Cuif (Fig. 4E-G) in sample JS221 (~248 m) confirms the Norian age of the upper unit (above ~239 m), consistent with its occurrence in the coeval Mailonggang Formation in Lhasa terrane (Xia and Liao, 1986).

Based on this integrated biostratigraphic evidence, we constrain the age of the upper Qulonggongba Formation to the Tuvalian 2 (Middle Tuvalian) and the overlying Qimala Formation to the Tuvalian 2–Lacian (Late Carnian–Early Norian), spanning the interval from ~233 Ma to ~227 Ma (Ogg et al., 2020).

5. Carbonate microfacies

5.1. Microfacies analysis

In this study, a total of eight microfacies types (MF1–MF8), representing three sedimentary environments, were identified in the upper Qulonggongba and Qimala Formations of the Jiesheng Section.

5.1.1. MF1 Sandy micrite

MF1 is extensively distributed in the upper Qulonggongba Formation. In outcrop, it appears as yellow, thin- to medium-bedded horizons susceptible to weathering, locally intercalated with thin, argillaceous layers (Fig. 4A-B). MF1 mainly comprises abundant terrigenous grains floating in the micritic matrix (Fig. 5A). Terrigenous components include fine-silty, well-sorted, angular to subangular quartz (10–30%), mica (<10%), and minor feldspar. Bioclasts are rare (<10%) and mostly bivalves (Fig. 5B). Laminar mica exhibits a weak directional alignment in thin sections. The matrix is dominated by generally recrystallized micrite, with a small amount of clay and dark flocculent organic matter.

The low compositional and textural maturity, coupled with the abundance of quartz, feldspar, and mica, indicates a depositional setting within the landward zone of a protected inner ramp strongly influenced by proximal terrigenous influx. This low-energy setting inhibited the winnowing of micrite and facilitated the preservation of organic matter alongside alternating continuous argillaceous laminae.

5.1.2. MF2 Sandy bioclastic wackestone

MF2 occurs sporadically within the lower-middle interval of the upper Qulonggongba Formation. It is characterized by fine-grained quartz (10–20%) and bioclasts (10–20%), including bivalves, echinoderms, and foraminifera (Fig. 5C-D). The matrix consists of micrite and clay. Most bioclasts (bivalves and echinoderms) are fragmented and exhibit weak directional alignment.

The fragmented and aligned bioclasts suggest transport by wave-induced currents. Although the high terrigenous content indicates continued proximity to a clastic source, the micrite matrix suggests deposition still occurred in a protected inner ramp setting. This environment was likely situated slightly seaward and received both terrigenous influx from the land and bioclastic input from the open sea (Flügel, 2010).

5.1.3. MF3 Bioclastic floatstone

MF3 is mainly characterized by a matrix-supported texture and sporadically distributed in the upper Qulonggongba Formation. Bioclasts are the dominant carbonate grains (10–20%; Fig. 5E), with bivalves (>2 mm) being the most abundant, accompanied by minor ostracods, crinoids, and gastropods. The matrix is micritic calcite with minor fine-grained quartz (<5%).

MF3 is characterized by abundant bioclasts, poor sorting, and a dominance of bivalves as the primary bioclastic component. Combined with sparse bioturbation, MF3 points to a low-energy inner ramp environment with normal salinity and moderate water circulation.

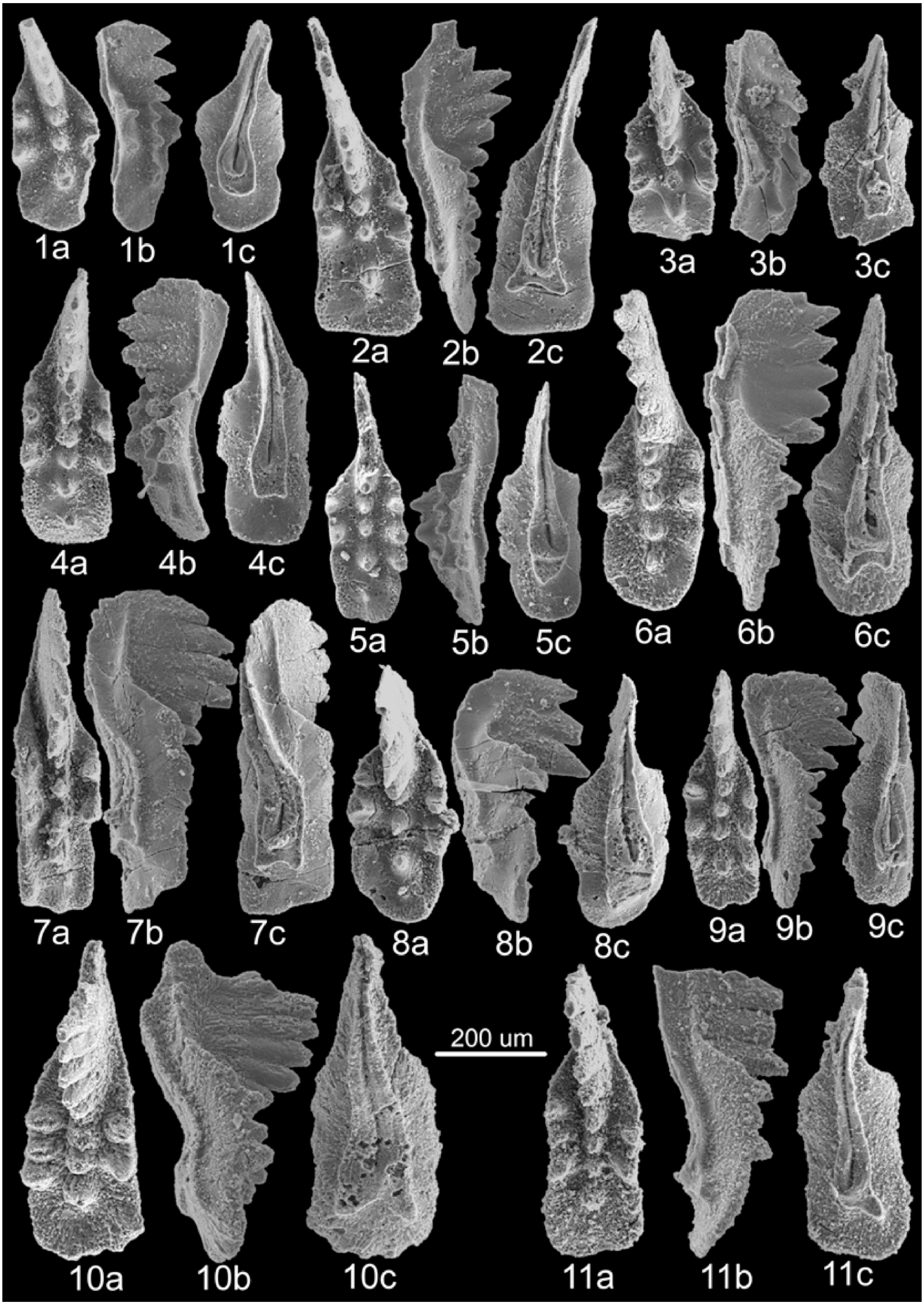

Fig. 2. Scanning electron microscope (SEM) images of conodonts from Jiesheng Section 1. *Carnepigondolella pseudoechinata*, JS204; 2. *Ancyrogondolella quadrata*, JS214; 3. *Primatella* aff. *orchardi*, JS214; 4. *Carnepigondolella pseudoechinata*, JS214; 5. *Carnepigondolella* cf. *zoae*, JS214; 6. *Primatella subquadrata*, JS244; 7. *Metapolygnathus communisti*, JS214; 8. *Mockina* aff. *Medionorica*, JS214; 9. *Metapolygnathus mersinensis*, JS244; 10. *Ancyrogondolella quadrata*, JS244; 11. *Metapolygnathus mersinensis*, JS214.

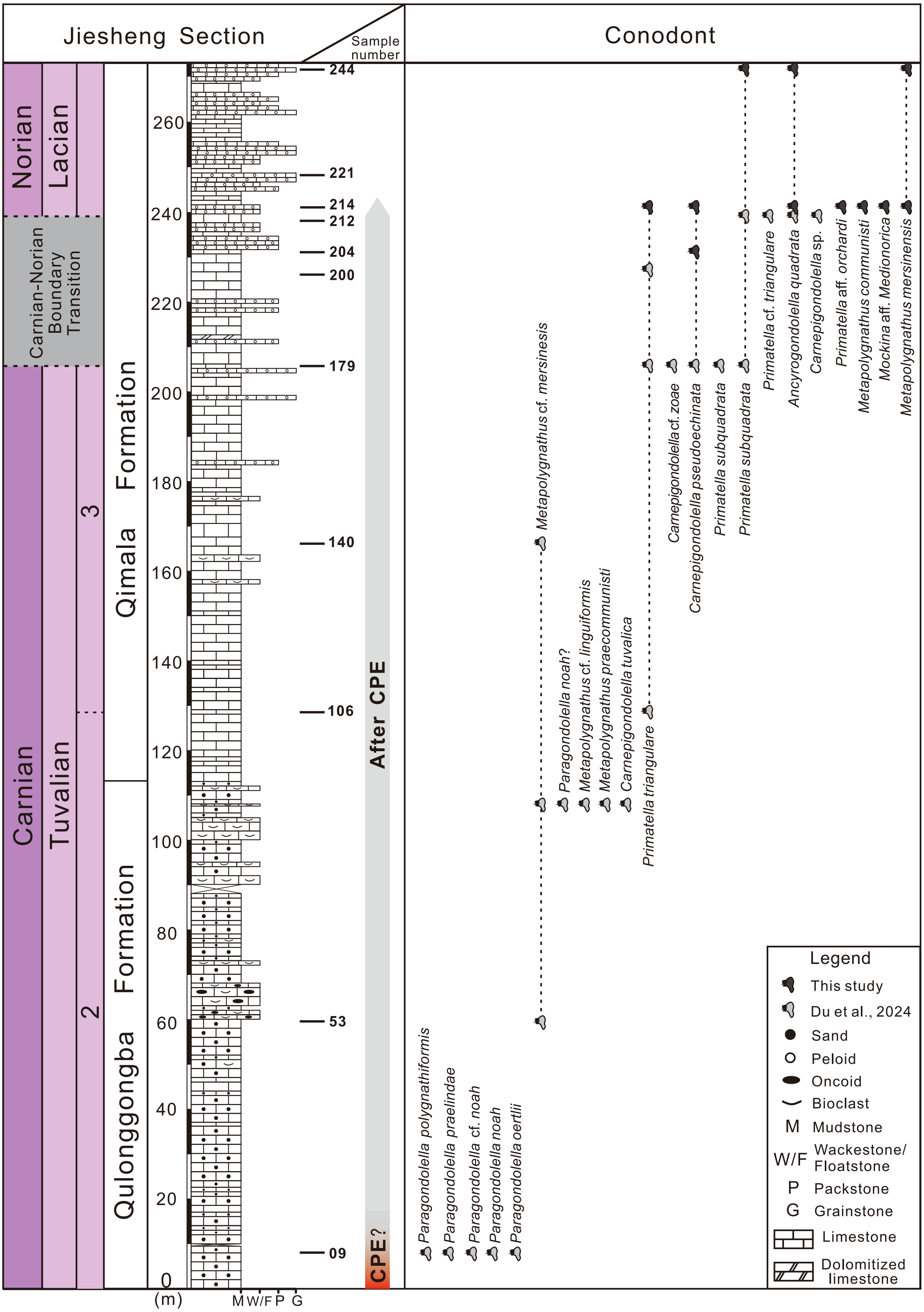

Fig. 3. Lithostratigraphic column and conodont distribution of Jiesheng section.

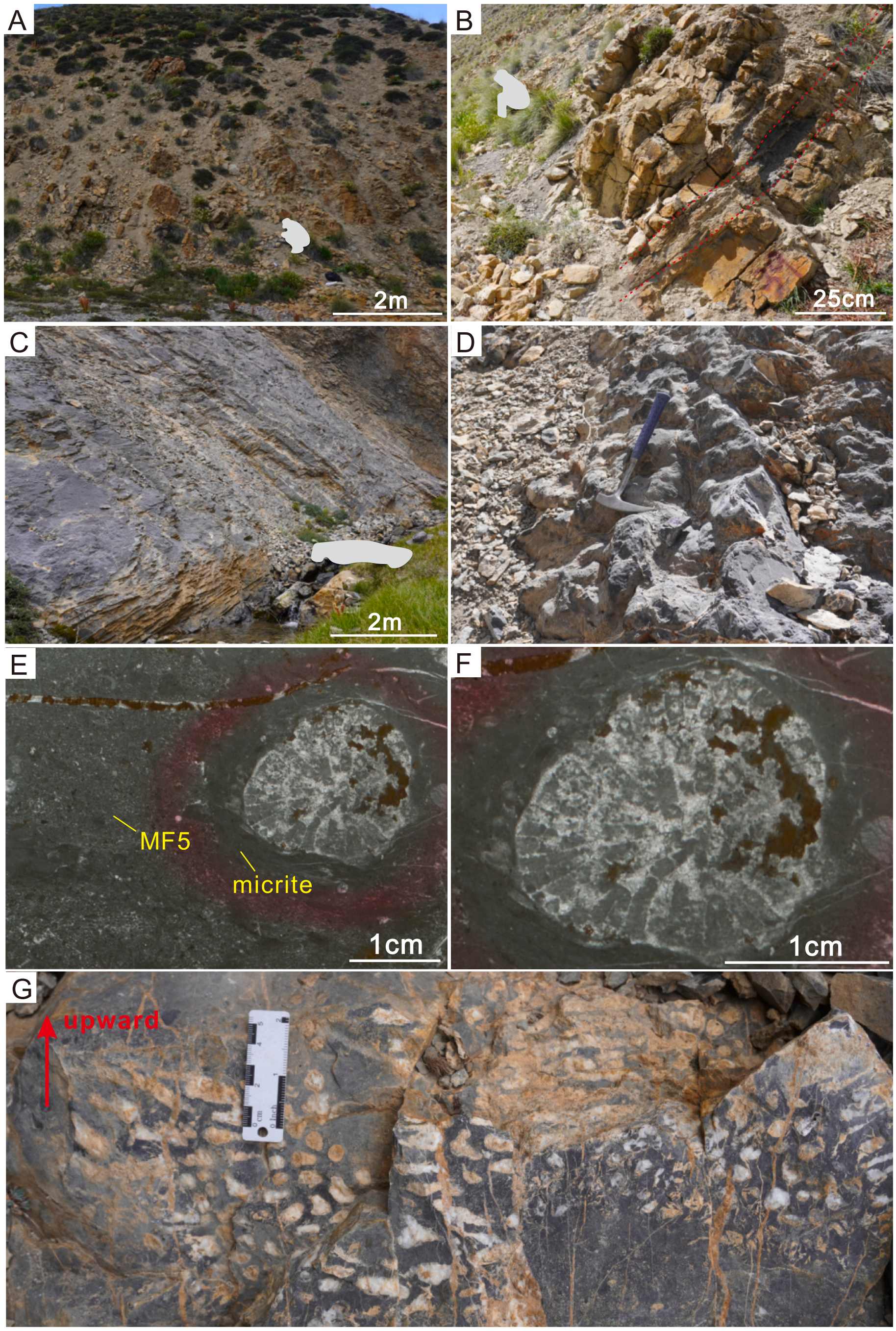

Fig. 4. Field photographs and thin-section photomicrographs. (A) Yellow mixed siliciclastic-carbonate rock of the upper Qulonggongba Formation; (B) Thin-bedded interlayers within the upper Qulonggongba Formation; (C) Limestone of the Qimala Formation; (D) Nodular limestone in the lower Qimala Formation; (E) and (F) Thin-section photos of coral *Retiophyllia* type IV Cuif; (G) *Retiophyllia*-bearing limestone. (For interpretation of the references to colour in this figure legend, the reader is referred to the web version of this article.)

5.1.4. MF4 Bioclastic-oncoidal wackestone

MF4 is sporadically distributed in the upper Qulonggongba Formation and is characterized by a matrix-supported texture. The grain assemblage is poorly sorted and comprises a mixture of bioclasts (10–15%), oncoids (10–15%), minor peloids and silty-sized quartz (<5%) embedded in a micritic matrix (Fig. 5F). The bioclasts are dominated by shallow-marine fauna such as bivalves and echinoderms, with rare ostracods and brachiopods. A significant proportion of these skeletal grains displays micritic envelopes, which were grown around grains prior to final burial. Besides, oncoids are also presented within matrix. They are irregular to sub-rounded in shape, composed predominantly of micritic calcite, and encapsulate fine bioclastic grains or several silt-sized quartz grains.

The abundance of micritic oncoids indicates the widespread microbial bonding that integrates bioclasts, quartz and microbially induced precipitation of micrite. The chaotic distribution of coarse and irregular grains within a micritic matrix indicates that wave action crushed and transported oncoids from relatively high-energy shoals to quieter areas. This microfacies can probably be formed within the low-energy environments of the inner ramp.

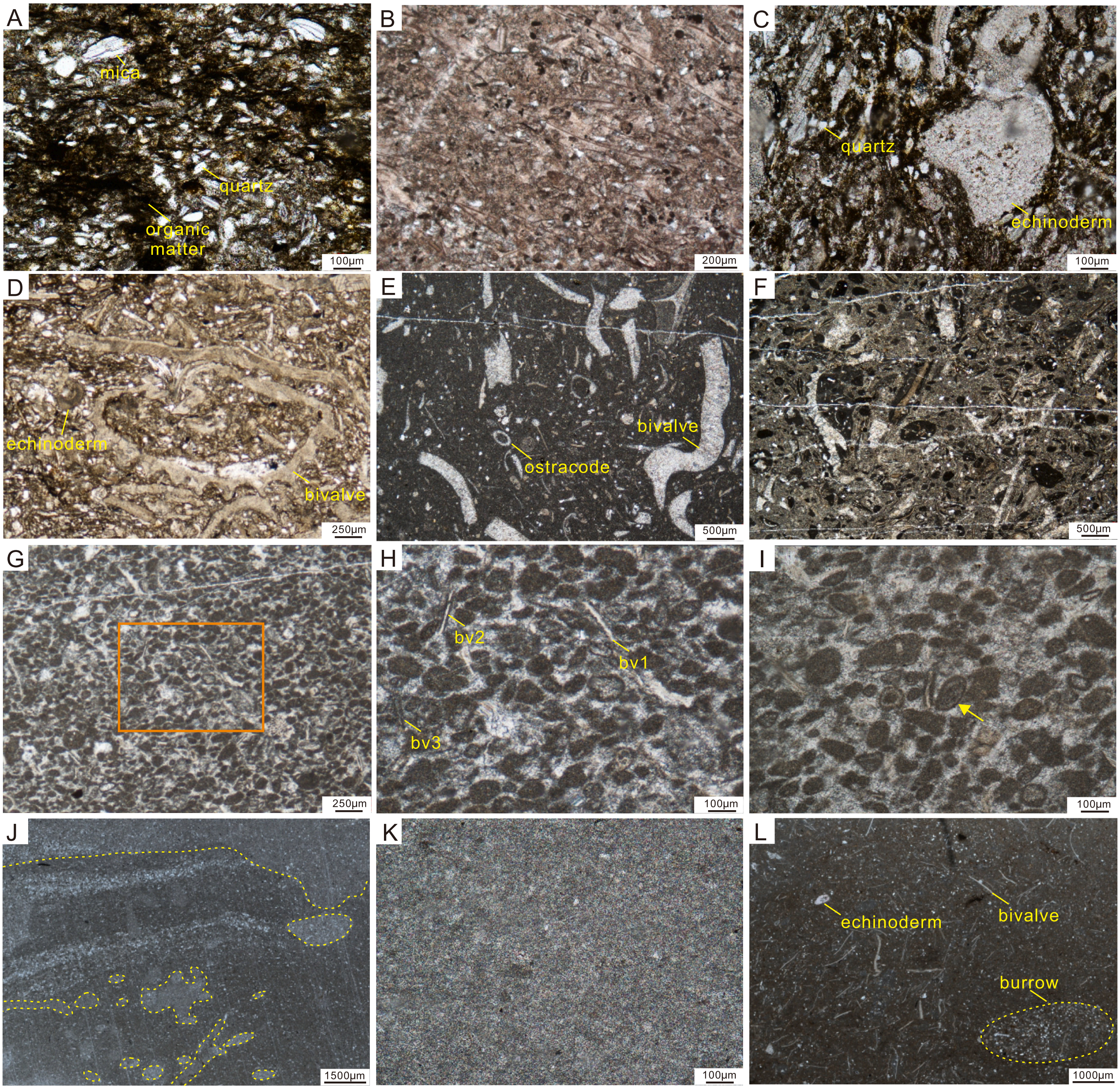

Fig. 5. Photomicrographs of microfacies types. (A) and (B) MF1 Sandy micrite; (C) and (D) MF2 Sandy bioclastic wackestone; (E) MF3 Bioclastic floatstone; (F) MF4 Bioclastic-oncoidal wackestone; (G) MF5 Peloidal packstone/grainstone. Orange rectangle represents the extent of (H); (H) MF5 Peloidal packstone/grainstone. bv1-bivalve, bv2-partly micritized bivalve, bv3-completely micritized bivalve; (I) MF5 Peloidal packstone/grainstone. Yellow arrow indicates the nearly complete micritization of a foraminifer; (J) MF6 Bioturbated mudstone/wackestone; (K) MF7 Mudstone; (L) MF8 Bioclastic wackestone. (For interpretation of the references to colour in this figure legend, the reader is referred to the web version of this article.)

5.1.5. *MF5 Peloidal packstone/grainstone with micritic limestone*

MF5 dominates the upper part of Qimala Formation. Peloidal packstone/grainstone is dominated by fine-grained peloids and alternates with pure micritic limestone. Bioclasts are a subordinate component (<10%) of peloidal packstone/grainstone, primarily comprising echinoderms, bivalves, foraminifers and ostracods. Terrigenous content is low and only locally present (<5%). The matrix is predominantly composed of sparry calcite (Fig. 5G-I). Additionally, the scleractinian coral *Retiophyllia* type IV Cuif is found in MF5 (Fig. 4E-G; sample JS221, ~248 m). The coral fossil is surrounded by a uniform micritic coating (<0.5 mm thick), while the outer surrounding sediment remains a peloidal grainstone cemented by sparry calcite (Fig. 4E).

The peloids found in MF5 are spherical, ellipsoidal to subangular in shape and 50–200 μm in size. Most of peloids are composed of micritic calcite, exhibiting indistinct internal microstructures, weak morphological variation and definite margins (Fig. 5G-I). Diagnostic features typical of microbial-derived peloids (e.g., cloudy-looking nuclei, diffuse margins, microbial filamentous remains, or clotted cluster shapes; Adachi et al., 2004; Yan et al., 2019) are notably absent. Bioclasts can be observed at various stages of micritization, eventually degrading completely into micritic grains (Fig. 5I), which constitute a significant supply of peloids found in this section. The consistent co-occurrence of peloids with partially micritized bioclasts, along with their relatively large size (mostly >50 μm compared to typical <20 μm microbial peloids; Chafetz, 1986), strongly suggests a skeletal/metazoan rather than microbial origin for these peloids. In addition, few peloids with bigger size (150–200 μm) and significantly irregular shape can probably be derived from the mechanical fragmentation of carbonate mud.

The grain-supported texture of the peloidal grainstone, paucity of depositional micrite, and dominance of well-defined peloidal grains suggest episodic winnowing under moderate- to relatively high-energy conditions in a shallow inner-ramp setting. In contrast, the frequent intercalation of micritic limestone records periods or localized areas of reduced hydrodynamic energy. We therefore interpret MF5 as representing a shallow inner-ramp shoal–back-shoal system characterized by pronounced small-scale spatial and/or temporal variations in hydrodynamic conditions.

The occurrence of *Retiophyllia* type IV Cuif within MF5 is consistent with such environmental heterogeneity. Although the photosymbiotic status and precise depth preference of Triassic scleractinian corals cannot be confidently constrained, *Retiophyllia* has previously been documented from shallow-water carbonate-platform and reef–lagoon settings. The coral colony in the studied section is surrounded by a thin, relatively uniform micritic coating, whereas the adjacent sediment consists of spar-cemented peloidal grainstone, suggesting that the coral occupied a localized microenvironment distinct from the surrounding grain-dominated substrate. We therefore interpret its occurrence as evidence for localized coral colonization in a relatively protected, lower-energy back-shoal habitat (Bernecker et al., 1999), possibly forming a small coral buildup, rather than using the coral itself as an independent indicator of photic-zone water depth.

5.1.6. MF6 Bioturbated mudstone/wackestone

MF6 is sporadically distributed in the lower-middle part of the Qimala Formation. This microfacies is mainly composed of micritic calcite and distinguished by intense bioturbation, which disrupts the original sedimentary fabric. Burrows are typically filled with microsparite, well-sorted silty quartz and bioclasts, contrasting with the surrounding micritic matrix. Additionally, irregular, millimeter-scale burrow-mottled bedding or bioturbation interfaces are locally preserved within the sequence (Fig. 5J).

The extensive bioturbation indicates an oxygenated seafloor with weak wave agitation, where burrows produced by benthic organisms were rapidly filled and preserved by siliciclastic and carbonate sediments. Consequently, MF6 represents the lowermost part of the middle ramp that is located close to or just below the storm wave base (SWB).

5.1.7. MF7 Mudstone

MF7, the most representative facies in the lower part of the Qimala Formation, consists of thin- to medium-bedded, locally nodular micritic limestone (Fig. 4C-D). The matrix is almost exclusively micrite with very minor dispersed silt or fine-grained bioclasts (<10%, Fig. 5K).

The absence of coarse terrestrial and carbonate grains, and the dominance of micrite indicate a low-energy outer ramp environment (Seyedmehdi et al., 2016).

5.1.8. MF8 Bioclastic wackestone

This microfacies is sporadically distributed in the lower-middle part of Qimala Formation and characterized by higher bioclastic abundance (10–20%) compared to the inner ramp facies. The fossil assemblage includes filamentous thin-shelled bivalves, echinoderms, ostracods, and brachiopods (Fig. 5L). The bioclasts are generally well-sorted but fragmented. The matrix consists predominantly of micritic calcite with negligible terrigenous materials (<5%).

The increased fossil abundance suggests an open-marine environment with efficient water circulation. The dominance of lime mud and the presence of thin-shelled organisms suggest deposition occurred in a low-energy setting like an outer ramp (Fucelli et al., 2023).

5.2. Quantitative grain composition

Quantitative grain statistics reveal that terrigenous components are ubiquitous throughout the upper Qulonggongba Formation. Their abundance typically ranges from 10% to 25% (average 15.4%, $n = 92$), with a maximum peak of ~50% at the basal interval. Bioclasts are generally sparse and sporadically distributed within this formation; they consistently account for less than 20% of the volume, although a slight upward-increasing trend in both frequency and abundance is observed up-section. In sharp contrast, the overlying Qimala Formation is characterized by a significant reduction in terrigenous input, averaging only 1.5%. Most samples contain less than 10% terrigenous material, with values diminishing to near-zero towards the top of the formation. While bioclastic content remains low (average 0.7%, $n = 153$), peloids become a major constituent (average 7.4%, $n = 153$). Notably, peloid abundance exhibits a marked increase in the upper Qimala Formation, reaching peak values of ~60–70% above the Carnian–Norian boundary (Fig. 6).

6. Discussion

6.1. Evolution of sedimentary environment

Integrated biostratigraphy and microfacies analysis reveal a distinct three-stage environmental evolution for the Jiesheng Section during the Tuvalian 2–Lacian interval. The succession documents a transition from a siliciclastic-influenced mixed system (the upper Qulonggongba Formation) to a carbonate-dominated ramp system (Qimala Formation), driven by changes in terrigenous influx and relative sea level.

During the Tuvalian 2 interval (~233–231 Ma), immediately following the end of the CPE, the upper Qulonggongba Formation was primarily deposited in a mixed siliciclastic-carbonate inner ramp setting, with sandy micrite (MF1) constituting the dominant microfacies. This microfacies reflects substantial terrigenous input, likely derived from intense weathering along the northern margin of the Indian continent. Against this backdrop, the sporadic occurrence of sandy bioclastic wackestone (MF2) with coarse skeletal grains indicates the intermittent development of high-energy hydrodynamic conditions, likely associated with storm-wave events. Towards the top of the formation, the appearance of bioclastic floatstone (MF3) and bioclastic-oncoidal wackestone (MF4) points to rapid relative sea-level fluctuations, marking a gradual transition from restricted landward side of inner ramp to seaward side (Fig. 7A).

During the Tuvalian 2–Lacian interval (~231–227 Ma), the deposition of the Qimala Formation marks a sharp reduction in terrigenous flux (Fig. 6). The basal interval is composed of mudstone (MF7), indicating a deepening-upward trend from an inner ramp to an outer ramp. In the middle Qimala Formation, the presence of bioturbated mudstone/wackestone (MF6), together with bioclastic wackestone (MF8), records the activities of living organisms. This period corresponds to a middle-outer ramp setting with improved water circulation, which fostered the proliferation of open-marine fauna and extensive bioturbation. Above this interval, an obvious relative sea level fall caused a shift in depositional environment from the middle-outer ramp to an inner ramp, where peloidal packstone/grainstone with micritic limestone (MF5) was deposited (Fig. 7B). In the nearby Spiti area, the resurgence of carbonate production after the CPE also occurred and was characterized by the deposition of coral limestone and peloidal limestone (Bhargava et al., 2004; Hornung et al., 2007b).

Microfacies analysis integrated with biostratigraphy enables reconstruction of the post-CPE sedimentary evolution in the Tibetan Himalaya. Inner-ramp environments influenced by terrigenous input and hydrodynamics variations in Tuvalian 2 transitioned upward to the middle-outer ramp settings in Tuvalian 3, and subsequently to inner-ramp environment during the Lacian (Fig. 6).

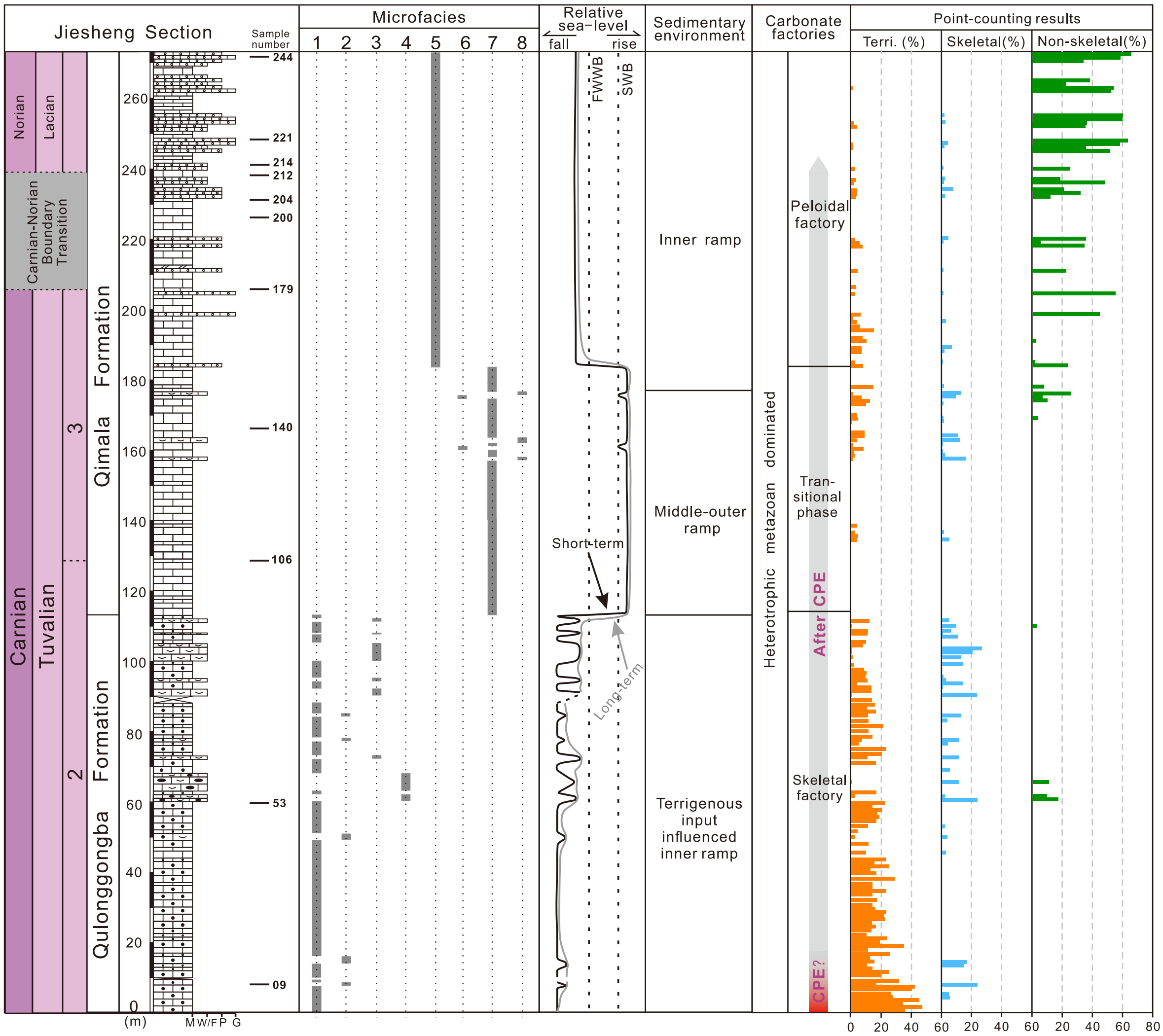

Fig. 6. Vertical distribution of sedimentary microfacies, relative sea-level change and quantitative grain composition results of the Jiesheng Section. Abbreviations: FWWB: Fair-weather wave base; SWB: Storm wave base; Terri. = Terrigenous grains; Skeletal = Skeletal grains; Non-skeletal = Non-skeletal grains.

6.2. *Carbonate factory transition and controlling factors*

6.2.1. *Evolution of carbonate factory*

Applying the process–product approach, we identify three distinct evolutionary stages of carbonate producers and production in the Jiesheng Section (western Tibetan Himalaya), driven by changing environmental conditions during the Tuvalian 2–Lacian interval.

Stage 1, Tuvalian 2 interval (the upper Qulonggongba Formation, ~233–231 Ma): Stressed heterotrophic metazoan skeletal factory. Although carbonate production was biologically controlled by shallow-marine heterotrophs (mainly bivalves and echinoderms), their skeletal remains are subordinate to terrigenous clasts (MF1, MF2). The low abundance and diversity suggest that high water turbidity and nutrient flux, driven by intense terrigenous input, suppressed carbonate producers and thus its production, restricting the factory to a small-scale assemblage of stress-tolerant taxa. In summary, this stage represents a low-productivity heterotrophic metazoan skeletal factory (hereafter: Skeletal Factory). Throughout this and subsequent stages, the voluminous carbonate lime mud characterizing the succession was likely significantly contributed by intense bioerosion, micro-boring, and the subsequent mechanical fragmentation of locally abundant metazoan skeletons. This biological and physical breakdown of weakened skeletons provided a continuous supply of carbonate mud to the protected inner to middle ramp.

Stage 2, Tuvalian 2–Tuvalian 3? (lower to middle Qimala Formation, ~231–229 Ma): Transitional skeletal factory. The waning terrigenous influx of this stage (MF6, MF7, and MF8; Fig. 6) improved water clarity and stability, leading to increased bioturbation. However, the fundamental factory type remained unchanged; heterotrophic metazoans continued to dominate, and bioclasts remained the primary carbonate grain type. Carbonate production efficiency remained low, and the system had not yet transitioned to a fundamentally different production mode.

Stage 3, Tuvalian 3?–Lacian (upper Qimala Formation, ~229–227 Ma): Peloidal Factory. This unit is dominated by peloidal packstone/grainstone with micritic limestone (MF5), notably devoid of microbial binding textures (e.g., thrombolites). While heterotrophic metazoans remained the primary producers, the dominant product shifted from skeletal grains to peloids. Although quantitative grain analysis shows a decrease in identifiable skeletal grains during this stage (Fig. 6), this does not reflect a decline in metazoan abundance. Instead, from a "process-product" perspective, the dramatic increase in peloids (reaching 60–70%) represents a fundamental shift in the preservation state of the carbonate products. The high primary productivity of metazoans was continuously masked by intense biological processing (i.e., complete micritization of skeletons) and physical fragmentation. These peloids predominantly originated from the complete micritization of bioclasts (e.g., bivalves and echinoderms), coupled with the physical

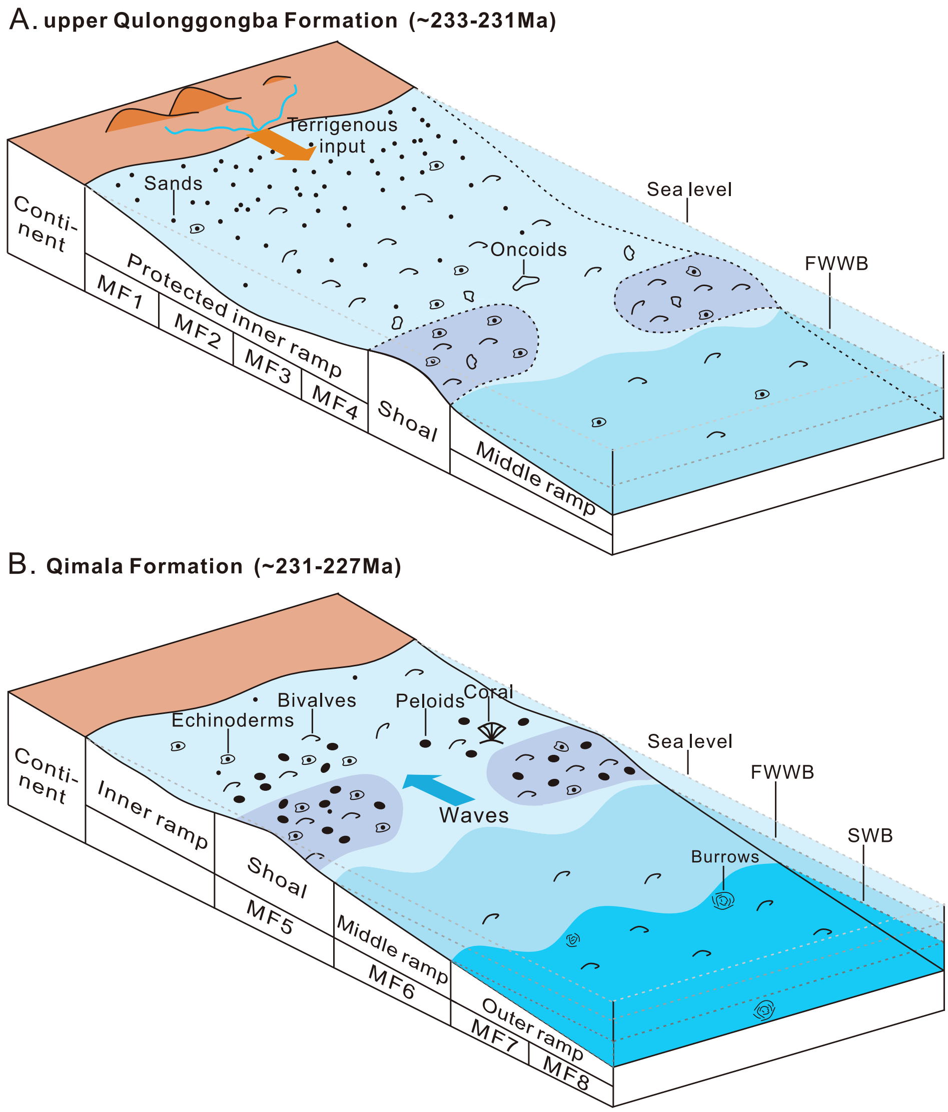

Fig. 7. Depositional models and microfacies distribution. (A) Mixed siliciclastic–carbonate inner ramp system (the upper Qulonggongba Formation). (B) Carbonate-dominated ramp system (the Qimala Formation).

fragmentation of bio-eroded carbonate mud generated by metazoan metabolism (Pomar, 2020).

These peloids were subsequently transported into protected inner-ramp back-shoal settings. The high-frequency interbedding of low-energy micritic limestone and relatively high-energy peloidal packstone/grainstone (MF5) indicates that these high-productivity carbonate shoals were highly mobile, frequently migrating in response to relative sea-level fluctuations without shutting down the factory. Importantly, these interbedded limestones exhibit parallel bedding and completely lack diagnostic tempestite or calciturbidite structures (e.g., hummocky cross-stratification, current ripples, or Bouma sequences). Furthermore, the discovery of well-preserved scleractinian corals (*Retiophyllia* type IV Cuif) within the MF5 facies (Fig. 4E-G) strictly precludes an outer-ramp or basinal origin, firmly validating a shallow protected inner-ramp setting. Notably, although the Early Norian scleractinian coral *Retiophyllia* type IV Cuif, likely representing a small coral colonization (Fig. 4E-G), was found in sample JS221, the absence of photoautotrophic organisms (e.g., calcareous green algae) indicates that the factory remained dominated by heterotrophs (Reijmer, 2021). Therefore, despite the shift in dominant grain type (from skeletal to peloidal), the system was still driven by heterotrophs, with marine conditions remaining unsuitable to support the large-scale proliferation of photoautotrophic or microbial communities.

6.2.2. *Controlling factors of carbonate factory transition*

Relative sea-level (RSL) fluctuations fundamentally influence carbonate factories by modifying sedimentary accommodation space (Pomar, 2001). Specifically, sea-level drop may lead to platform exposure, whereas sea-level rise can increase water depth and reduce the light intensity reaching the seafloor, potentially affecting in-situ carbonate production. However, given the mobility of carbonate-producing organisms, such RSL changes typically induce lateral migrations of facies belts rather than a complete reorganization of the carbonate factory. A fundamental shutdown or turnover of a factory generally requires the significant deterioration of key ecological factors (Schlager, 1999; Pomar, 2001). In the western Tibetan Himalaya, the RSL curve for the Tuvalian 2–Lacian period exhibits continuous and moderate-amplitude variations (Fig. 6). Although the transition from the heterotrophic skeletal factory to the peloidal factory coincides with a RSL fall, this correlation is insufficient to implicate RSL as the primary driver. Crucially, during the preceding early to middle Tuvalian 2 interval, the section experienced an overall RSL rise, consistent with global eustatic trends (Haq, 2018), yet the carbonate factory type remained unchanged. Therefore, relative sea-level changes were not the dominant factor controlling the observed transition of the carbonate factory here.

Instead, we identify variations in terrigenous influx and the associated changes in nutrient levels and water turbidity as the dominant control on carbonate producers and thus carbonate factory evolution in the study area. Heterotrophic organisms (such as bivalves, foraminifera, and echinoderms) generally thrive in mesotrophic to eutrophic conditions (Mutti and Hallock, 2003). During Stage 1, intense terrigenous input likely delivered abundant nutrients, theoretically supporting these heterotrophs. However, the associated high turbidity and siliciclastic sedimentation rates significantly inhibited carbonate production and the preservation of skeleton (Reijmer, 2021). Consequently, although heterotrophs were present, the factory was suppressed, resulting in a low-productivity system where skeletal grains were subordinate to siliciclasts. In contrast, during Stage 3, the substantial reduction in terrigenous input led to clearer water conditions. While nutrient level likely decreased relative to Stage 1, it remained sufficient to support the heterotrophic community. Besides, the removal of turbidity stress allowed carbonate production efficiency to surge. The widespread formation of peloids during this stage reflects a high-efficiency carbonate system that was no longer hindered by clastic interference.

Overall, the evolution of carbonate factories in the western Tibetan Himalaya was governed by the magnitude of terrigenous flux. During the early post-CPE interval (Stage 1), intense terrigenous input provided nutrients for heterotrophs, while suppressing calcification through increasing turbidity. As the influence of terrigenous input waned (Stages 2–3), the factory gradually recovered from environmental stress, allowing the established heterotrophic community to maximize its production efficiency, ultimately manifesting as a high-productivity peloidal factory.

6.3. Comparison of post-CPE carbonate factory transformations

To assess the global universality of post-CPE recovery patterns, we compared the carbonate-platform evolutionary history of western Tibetan Himalaya with well-documented records from Italy (Dolomites and Julian Alps; Roghi et al., 2010; Dal Corso et al., 2012, 2015, 2018; Caggiati et al., 2018) and South China (Sichuan Basin, Jin et al., 2018, 2019, 2020; Fig. 8A). Due to the incomplete carbon isotope records,

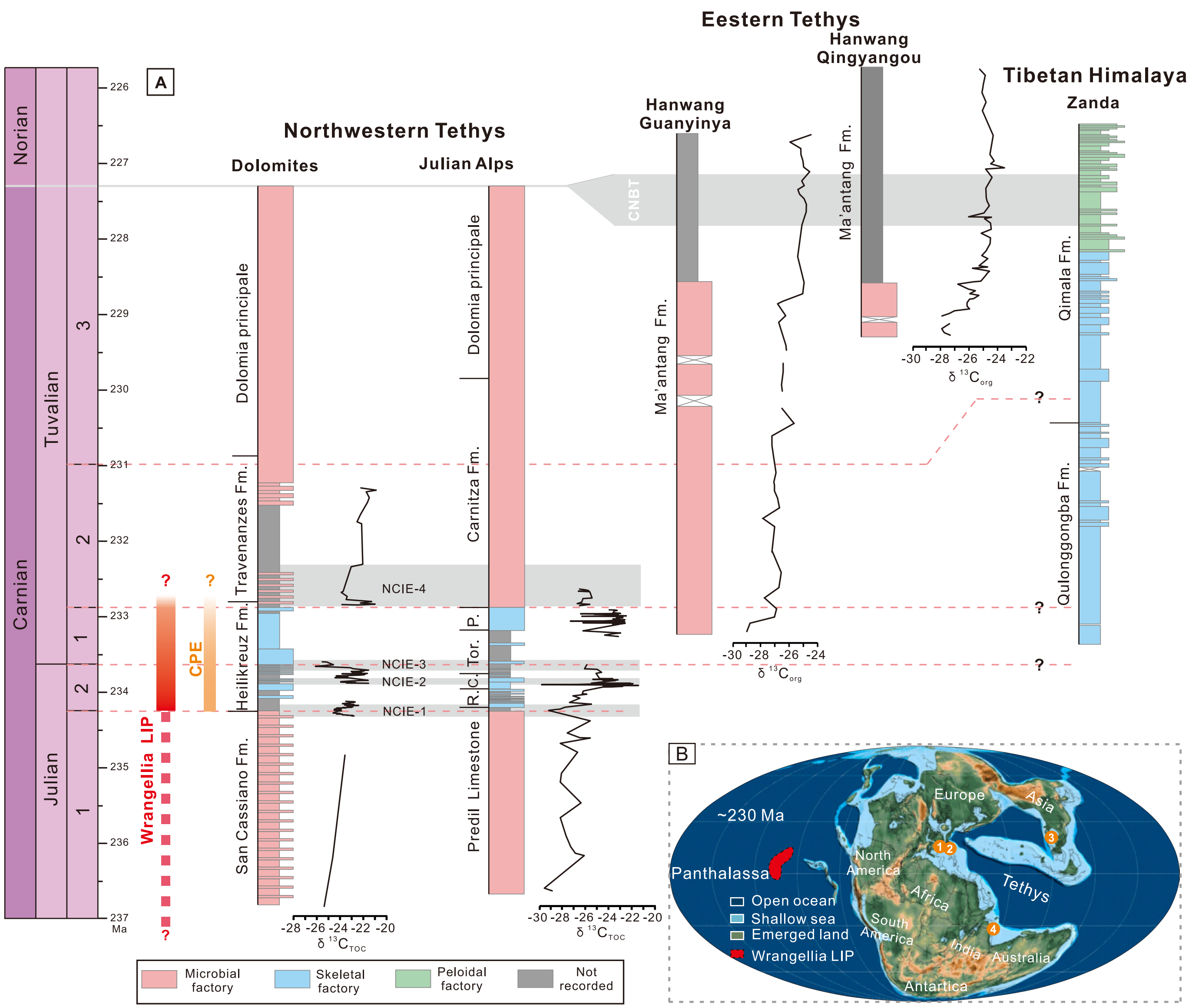

Fig. 8. (A) Comparison of carbonate factory evolution among Italy, the Sichuan Basin, and the western Tibetan Himalaya. Data sources: Italy (Roghi et al., 2010; Dal Corso et al., 2012, 2015, 2018; Caggiati et al., 2018); Sichuan Basin (Jin et al., 2018, 2019, 2020). (B) Paleogeographic map of the Late Triassic (modified after Scotese and Schettino, 2017). 1: Dolomites; 2: Julian Alps; 3: Sichuan Basin; 4: Zanda. Abbreviations: R. = Rio del Lago Formation; C. = Conzen Formation; Tor. = Tor Formation; P. = Portella Limestone; CNBT = Carnian–Norian Boundary Transition.

however, biostratigraphy for each section is also used as the primary basis for comparison. A synthesis of biostratigraphic and sedimentological data reveals a distinct divergence in the post-CPE recovery patterns between the Tibetan Himalaya and other Tethyan regions.

6.3.1. *Regional disparity of post-CPE carbonate factory patterns*

In Italy, a transition from the skeletal factory to the microbial factory occurred in the Early Tuvalian 2, shortly after the CPE (Dal Corso et al., 2015, 2018; Jin et al., 2020; Fig. 8A). These microbial carbonates are ubiquitous across the platform: stromatolites and cyanobacterial fossils characterize the inner-platform settings, whereas in-situ microbial boundstones, thrombolites, oncoids, and pisoids dominate the outer-platform environments (Breda and Preto, 2011; Caggiati et al., 2018). A parallel trend is recorded in the Sichuan Basin, where the post-CPE interval saw a gradual expansion of microbial factories. Clustered peloidal micrite and reworked thrombolites occur in inner- to middle-ramp settings, while microbial carbonates dominate in-situ sponge mounds in outer-ramp environments (Jin et al., 2015, 2018, 2020; Shi et al., 2017). Although the transition in the Sichuan Basin appears to occur earlier (Tuvalian 1), this temporal discrepancy may stem from stratigraphic gaps or lower biostratigraphic resolution in those sections (Jin et al., 2019, 2020). In sharp contrast to the microbial dominance in Italy and the Sichuan Basin, the western Tibetan Himalaya maintained a heterotrophic skeletal factory dominance from the end of the CPE through the Tuvalian 2. Crucially, no microbial carbonates (e.g., stromatolites or thrombolites) have developed ubiquitously in this region. The subsequent transition during the Tuvalian 3–Lacian was to a peloidal factory, which was still driven by heterotrophic metazoans rather than microbial communities. Furthermore, while the Italian region developed flat-topped carbonate platforms, both the Sichuan Basin and the Zanda area evolved into carbonate ramp systems (Caggiati et al., 2018; Jin et al., 2019, 2020), demonstrating that microbial factories can thrive in diverse morphological settings (platforms, ramps, or isolated mounds) provided chemical conditions are favorable (Reijmer, 2021).

6.3.2. *Latitudinal and paleogeographic control on carbonate factories*

According to paleogeographic reconstructions, the Italian region and the Sichuan Basin were located in the northern tropical zone during the Late Triassic (Zhu et al., 1998; Tian et al., 2016; Scotese and Schettino, 2017; Fig. 8B). Conversely, the western Tibetan Himalaya was situated in the subtropical zone of the Southern Hemisphere (approx. 25–35°S). This latitudinal difference governed the physicochemical conditions of the seawater, providing a plausible explanation for the observed latitudinal heterogeneity in carbonate factory transitions. Conodont oxygen isotope data reveal two distinct warming pulses during the CPE, an initial increase of ~3 °C and a subsequent rise of ~6 °C, corresponding to the first and third negative carbon isotope excursions, respectively (Dal Corso et al., 2020). These elevated temperatures persisted even after the termination of the CPE. High surface seawater temperatures (SST) and elevated carbonate saturation states in the low-latitude tropical regions were favorable for the rapid calcification of microbial communities. This interpretation aligns with modern observations where microbial and abiotic precipitate-rich systems (e.g., the Persian Gulf) are predominantly found in high-temperature tropical regions (Laugié et al., 2019). Despite the global post-CPE warmth, the subtropics maintained lower SST and carbonate saturation states than the tropics due to the latitudinal gradient. In the subtropical western Tibetan Himalaya, the relatively cooler SSTs likely did not exceed the lethal thermal thresholds of benthic fauna. Consequently, this region served as a habitable refugium for metazoans. The sustained presence and active bioturbation of these metazoan communities competitively excluded microbial mat development (i.e., preventing a "disaster taxa" microbial takeover). Furthermore, compared to the tropics, this subtropical setting maintained lower carbonate saturation states, which are less favorable for rapid microbial calcification but sufficient for metazoans occupying diverse ecological niches. Therefore, the environment persistently favored a metazoan-dominated heterotrophic factory. This is consistent with modern carbonate factory distributions, where shallow-marine environments at latitudes above 30°N and 30°S are predominantly occupied by cold-water heterotrophic factories (Laugié et al., 2019).

Superimposed on the primary latitudinal control, the specific paleogeographic setting likely acted as an additional factor influencing carbonate factory evolution (Scotese and Schettino, 2017). Italy and the Sichuan Basin were situated in the southwestern and northeastern margins of the Tethys, respectively (Fig. 1). Unlike the western Tibetan Himalaya, these regions were relatively isolated from open ocean circulation. This relatively semi-restricted configuration often leads to a more stressed environment, which may have amplified the favorable tropical conditions for microbial factories known to thrive in stressed settings. In stark contrast, the Tibetan Himalaya was located on a passive continental margin directly facing the open Tethys and Panthalassa Ocean. This configuration ensured efficient water exchange, maintaining stable, normal marine salinity and oxygenation. We propose that this open-marine stability reinforced the subtropical exclusion of microbial communities, thereby precluding a microbial takeover.

7. Conclusion

Integrating conodont biostratigraphy and microfacies analysis, this study constrains the Jiesheng Section to the Tuvalian 2–Lacian interval (Late Carnian–Early Norian), representing the recovery phase following the Carnian Pluvial Episode (CPE). The sedimentary evolution documents a distinct transition from a mixed siliciclastic–carbonate inner ramp system (the upper Qulonggongba Formation) to a carbonate middle-to-outer ramp setting (the Qimala Formation). The evolution of carbonate factories was primarily controlled by the intensity of terrigenous influx. During the Tuvalian 2, high terrigenous input created a nutrient-rich yet turbid environment, resulting in a suppressed skeletal factory. As terrigenous influence waned in the Late Carnian, the carbonate factory transitioned to a peloidal factory, representing a surge in production efficiency due to improved water clarity. In contrast, relative sea-level changes likely played a secondary role, primarily inducing lateral facies migration.

Distinct from the microbial-dominated recovery pattern observed in the tropical, semi-restricted basins in Italy and South China, the subtropical Tibetan Himalaya retained a heterotrophic metazoan-dominated system throughout the post-CPE interval. We attribute this divergence primarily to latitudinal controls on seawater temperature and carbonate saturation, which were further amplified by paleogeographic configurations. The subtropical location set the baseline physicochemical conditions that inhibited rapid microbial calcification. Superimposed on this gradient, the open-marine setting on the passive continental margin ensured stable, normal marine conditions that favored stenohaline metazoans over microbial communities. This study highlights that while the cessation of terrigenous stress is a prerequisite for carbonate recovery, the specific evolutionary trajectory (microbial versus skeletal) is ultimately governed by latitudinal controls, with paleogeographic configurations acting as a superimposed modulator.

CRediT authorship contribution statement

Tianhao Su: Writing – original draft, Methodology, Conceptualization. **Zhong Han:** Writing – review & editing, Supervision, Investigation, Funding acquisition, Conceptualization. **Yixing Du:** Writing – original draft, Methodology. **Jingxin Jiang:** Writing – review & editing. **Xiumian Hu:** Writing – review & editing, Funding acquisition, Conceptualization.

Declaration of competing interest

The authors declare that they have no known competing financial interests or personal relationships that could have appeared to influence the work reported in the paper.

Acknowledgements

We thank Jiawei He and Chunrun Liu for their assistance in fieldwork, and Xia Wang for help with coral photography. We extend our sincere gratitude to Weihua Liao and Yiwei Xu for their assistance with coral identification and constructive suggestions, respectively. We are grateful to Prof. Nereo Preto and another anonymous reviewer, whose comments and suggestions greatly improved this manuscript. This research was supported by the National Natural Science Foundation of China (Grant No. 42272116) and the National Key Research and Development Program of China (Grant No. 2023YFF0804000). This paper is a contribution to IGCP Project 739.

Appendix A. Supplementary data

Supplementary data to this article can be found online at https://doi.org/10.1016/j.palaeo.2026.114173.

Data availability

The authors confirm that all data necessary for supporting the scientific findings of this paper have been provided.

References

Adachi, N., Ezaki, Y., Liu, J., 2004. The fabrics and origins of peloids immediately after the end-Permian extinction, Guizhou Province, South China. Sediment. Geol. 164, 161–178.
Appel, E., Müller, R., Widder, R., 1991. Palaeomagnetic results from the Tibetan Sedimentary Series of the Manang area (north central Nepal). Geophys. J. Int. 104, 255–266.
Bernecker, M., Weidlich, O., Flügel, E., 1999. Response of triassic reef coral communities to sea-level fluctuations, storms and sedimentation: evidence from a spectacular outcrop (Adnet, Austria). Facies 40, 229–279.
Bhargava, O.N., Krystyn, L., Balini, M., Lein, R., Nicora, A., 2004. Revised litho-and sequence stratigraphy of the Spiti Triassic. Albertiana 30, 21–39.
Brandano, M., Mateu-Vicens, G., Baceta, J., 2022. Understanding carbonate factories through palaeoecological and sedimentological signals – Tribute to Luis Pomar. Sedimentology 69, 5–23.
Breda, A., Preto, N., 2011. Anatomy of an Upper Triassic continental to marginal-marine system: the mixed siliciclastic–carbonate Travenanzes Formation (Dolomites, Northern Italy). Sedimentology 58, 1613–1647.
Caggiati, M., Gianolla, P., Breda, A., Celarc, B., Preto, N., 2018. The start-up of the Dolomia Principale/Hauptdolomit carbonate platform (Upper Triassic) in the eastern Southern Alps. Sedimentology 65, 1097–1131.
Chafetz, H.S., 1986. Marine peloids; a product of bacterially induced precipitation of calcite. J. Sediment. Res. 56, 812–817.
Dal Corso, J., Mietto, P., Newton, R., Pancost, R., Preto, N., Roghi, G., Wignall, P., 2012. Discovery of a major negative $\delta^{13}C$ spike in the Carnian (Late Triassic) linked to the eruption of Wrangellia flood basalts. Geology 40, 79–82.
Dal Corso, J., Gianolla, P., Newton, R., Franceschi, M., Roghi, G., Caggiati, M., Raucsik, B., Budai, T., Haas, J., Preto, N., 2015. Carbon isotope records reveal synchronicity between carbon cycle perturbation and the "Carnian Pluvial Event" in the Tethys realm (Late Triassic). Glob. Planet. Chang. 127, 79–90.
Dal Corso, J., Gianolla, P., Rigo, M., Franceschi, M., Roghi, G., Mietto, P., Manfrin, S., Raucsik, B., Budai, T., Jenkyns, H., Reymond, C., Caggiati, M., Gattolin, G., Breda, A., Merico, A., Preto, N., 2018. Multiple negative carbon-isotope excursions during the Carnian Pluvial Episode (Late Triassic). Earth Sci. Rev. 185, 732–750.
Dal Corso, J., Bernardi, M., Sun, Y., Song, H., Seyfullah, L., Preto, N., Gianolla, P., Ruffell, A., Kustatscher, E., Roghi, G., Merico, A., Hohn, S., Schmidt, A., Marzoli, A., Newton, R., Wignall, P., Benton, M., 2020. Extinction and dawn of the modern world in the Carnian (Late Triassic). Sci. Adv. 6, eaba0099.
De Zanche, V., Gianolla, P., Roghi, G., 2000. Carnian stratigraphy in the Raibl/Cave del Predil area (Julian Alps, Italy). Eclogae Geol. Helv. 93, 331–347.
Du, Y., Han, Z., Karádi, V., Su, T., Dong, J., Wu, Q., Guo, B., Sun, Y., Rigo, M., 2024. The conodont biostratigraphy of the upper Carnian (Upper Triassic) in the Tethys Himalaya area, South Tibet. Palaeogeogr. Palaeoclimatol. Palaeoecol. 651, 112387.
Dunham, R., 1962. Classification of carbonate rocks according to depositional texture: classification of carbonate rocks. In: Ham, W.E. (Ed.), Classification of Carbonate Rocks, 1. AAPG Mem., pp. 108–121
Embry, A.F., Klovan, J.E., 1971. A late Devonian reef tract on northeastern Banks Island, NWT. Bull. Can. Petrol. Geol. 19, 730–781.
Flügel, E., 2010. Microfacies of Carbonate Rocks: Analysis, Interpretation and Application, 2nd edn. Springer-Verlag, Berlin Heidelberg, pp. 1–984.
Fu, X., Wang, J., Wen, H., Wang, Z., Zeng, S., Song, C., Chen, W., Wan, Y., 2020. A possible link between the Carnian Pluvial Event, global carbon-cycle perturbation, and volcanism: new data from the Qinghai-Tibet Plateau. Glob. Planet. Chang. 194, 103300.
Fucelli, A., Golding, M., Peybernes, C., Martini, R., 2023. Siliciclastic input controlling carbonate deposition on a low-angle ramp system: new insight from the Upper Triassic Luning Formation (Western-Central Nevada). Sediment. Geol. 450, 106394.
Furin, S., Preto, N., Rigo, M., Roghi, G., Gianolla, P., Crowley, J., Bowring, S., 2006. High-precision U-Pb zircon age from the Triassic of Italy: implications for the Triassic time scale and the Carnian origin of calcareous nannoplankton and dinosaurs. Geology 34, 1009–1012.
Garzanti, E., 1999. Stratigraphy and sedimentary history of the Nepal Tethys Himalaya passive margin. J. Asian Earth Sci. 17, 805–827.
Gattolin, G., Preto, N., Breda, A., Franceschi, M., Isotton, M., Gianolla, P., 2015. Sequence stratigraphy after the demise of a high-relief carbonate platform (Carnian of the Dolomites): sea-level and climate disentangled. Palaeogeogr. Palaeoclimatol. Palaeoecol. 423, 1–17.
Greene, A., Scoates, J., Weis, D., Katvala, E., Israel, S., Nixon, G., 2010. The architecture of oceanic plateaus revealed by the volcanic stratigraphy of the accreted Wrangellia oceanic plateau. Geosphere 6, 47–73.
Haq, B., 2018. Triassic Eustatic Variations Reexamined, 28. GSA Today, pp. 4–9.
Hornung, T., Brandner, R., Krystyn, L., Joachimski, M., Keim, L., 2007a. Multistratigraphic constraints on the NW Tethyan "Carnian Crisis". N. M. Mus. Nat. Hist. Sci. Bull. 41, 59–67.
Hornung, T., Krystyn, L., Brandner, R., 2007b. A Tethys-wide mid-Carnian (Upper Triassic) carbonate productivity crisis: evidence for the Alpine Reingraben Event from Spiti (Indian Himalaya)? J. Asian Earth Sci. 30, 285–302.
Hu, X., Wang, J., Boudagher-Fadel, M., Garzanti, E., An, W., 2016. New insights into the timing of the India – Asia collision from the Paleogene Quxia and Jialazi formations of the Xigaze forearc basin, South Tibet. Gondwana Res. 32, 76–92.
Hu, X., Li, J., Han, Z., Li, Y., 2020. Two types of hyperthermal events in the Mesozoic–Cenozoic: environmental impacts, biotic effects, and driving mechanisms. Sci. China Earth Sci. 63, 1–18.
Jia, E., Corso, J.D., Wu, K., Du, Y., Wu, Y., Wang, F., Dai, X., Song, H., Chu, D., Zhong, L., Yuan, Z., Chen, X., Liu, Y., Li, Z., Song, H., 2025. Decoupling of $\delta^{13}C_{carb}$ and $\delta^{13}C_{org}$ during the Carnian Pluvial Episode in marine successions of South China. Chem. Geol. 695, 123053.
Jin, X., Ji, G., Shi, Z., Wang, Y., 2015. The sedimentary facies of Guanyinya Section in Hanwang, Mianzhu: implications for the environment evolution ahead of and after the Triassic Carnian Pluvial Event. Bull. Mineral. Petrol. Geochem. 34, 1173–1182 (In Chinese with English abstract).
Jin, X., Shi, Z., Rigo, M., Franceschi, M., Preto, N., 2018. Carbonate platform crisis in the Carnian (Late Triassic) of Hanwang (Sichuan Basin, South China): insights from conodonts and stable isotope data. J. Asian Earth Sci. 164, 104–124.
Jin, X., McRoberts, C.A., Shi, Z., Mietto, P., Rigo, M., Roghi, G., Manfrin, S., Franceschi, M., Preto, N., 2019. The aftermath of the CPE and the Carnian–Norian transition in northwestern Sichuan Basin, South China. J. Geol. Soc. Lond. 176, 179–196.
Jin, X., Gianolla, P., Shi, Z., Franceschi, M., Caggiati, M., Du, Y., Preto, N., 2020. Synchronized changes in shallow water carbonate production during the Carnian Pluvial Episode (Late Triassic) throughout Tethys. Glob. Planet. Chang. 184, 103035.
Ke, P., Fu, X., Peng, Q., Wei, H., Zeng, Y., Zhang, Q., Deng, J., 2023. Multiple carbon isotope excursions during the Carnian (Late Triassic) pluvial event: implications for global and regional perturbation. J. Geol. Soc. Lond. 180 jgs2022-168.
Keim, L., Spötl, C., Brandner, R., 2006. The aftermath of the Carnian carbonate platform demise: a basinal perspective (Dolomites, Southern Alps). Sedimentology 53, 361–386.
Klootwijk, C.T., Bingham, D.K., 1980. The extent of Greater India, III. Palaeomagnetic data from the Tibetan Sedimentary series, Thakkhola region, Nepal Himalaya. Earth Planet. Sci. Lett. 51, 381–405.
Laugié, M., Michel, J., Pohl, A., Poli, E., Borgomano, J., 2019. Global distribution of modern shallow-water marine carbonate factories: a spatial model based on environmental parameters. Sci. Rep. 9, 16432.
Lu, J., Zhang, P., Dal Corso, J., Yang, M., Wignall, P.B., Greene, S.E., Shao, L., Lyu, D., Hilton, J., 2021. Volcanically driven lacustrine ecosystem changes during the Carnian Pluvial Episode (Late Triassic). Proc. Natl. Acad. Sci. 118, e2109895118.
Lukeneder, S., Lukeneder, A., Harzhauser, M., İslamoğlu, Y., Krystyn, L., Lein, R., 2012. A delayed carbonate factory breakdown during the Tethyan-wide Carnian Pluvial Episode along the Cimmerian terranes (Taurus, Turkey). Facies 58, 279–296.
Mazza, M., Rigo, M., Gullo, M., 2012. Taxonomy and biostratigraphic record of the Upper Triassic conodonts of the Pizzo Mondello section (western Sicily, Italy), GSSP candidate for the base of the Norian. Riv. Ital. Paleontol. Stratigr. 118, 85–130.
Miller, C., Peterse, F., da Silva, A., Baranyi, V., Reichart, G., Kürschner, W., 2017. Astronomical age constraints and extinction mechanisms of the Late Triassic Carnian crisis. Sci. Rep. 7, 2557.
Mortensen, J., Hulbert, L.J., 1991. A U-Pb zircon age for a Maple Creek gabbro sill, Tatamagouche Creek area, southwestern Yukon Territory. In: Radiogenic Age and Isotopic Studies Report, 5, pp. 175–179.
Mount, J., 1985. Mixed siliciclastic and carbonate sediments: a proposed first-order textural and compositional classification. Sedimentology 32, 435–442.
Mueller, S., Krystyn, L., Kürschner, W.M., 2016. Climate variability during the Carnian Pluvial Phase — a quantitative palynological study of the Carnian sedimentary succession at Lunz am See, Northern Calcareous Alps, Austria. Palaeogeogr. Palaeoclimatol. Palaeoecol. 441, 198–211.
Mutti, M., Hallock, P., 2003. Carbonate systems along nutrient and temperature gradients: some sedimentological and geochemical constraints. Int. J. Earth Sci. 92, 465–475.

Ogg, J.G., Chen, Z.Q., Orchard, M.J., Jiang, H.S., 2020. Chapter 25 - The triassic period. In: Geologic Time Scale 2020. Elsevier, pp. 903–953.

Pecorari, M., Caggiati, M., Dal Corso, J., Cruciani, G., Tateo, F., Chu, D., Gianolla, P., 2023. Weathering and sea level control on siliciclastic deposition during the Carnian Pluvial Episode (Southern Alps, Italy). Palaeogeogr. Palaeoclimatol. Palaeoecol. 617, 111495.

Pomar, L., 2001. Ecological control of sedimentary accommodation: evolution from a carbonate ramp to rimmed shelf, Upper Miocene, Balearic Islands. Palaeogeogr. Palaeoclimatol. Palaeoecol. 175, 249–272.

Pomar, L., 2020. Chapter 12 - carbonate systems. In: Scarselli, N., Adam, J., Chiarella, D., Roberts, D.G., Bally, A.W. (Eds.), Regional Geology and Tectonics (Second Edition). Elsevier, pp. 235–311.

Pomar, L., Hallock, P., 2008. Carbonate factories: a conundrum in sedimentary geology. Earth Sci. Rev. 87, 134–169.

Preto, N., Hinnov, L.A., 2003. Unraveling the origin of carbonate platform cyclothems in the Upper Triassic Dürrenstein formation (Dolomites, Italy). J. Sediment. Res. 73, 774–789.

Preto, N., Willems, H., Guaiumi, C., Westphal, H., 2013. Onset of significant pelagic carbonate accumulation after the Carnian Pluvial Event (CPE) in the western Tethys. Facies 59, 891–914.

Ran, B., Wang, C.S., Zhao, X.X., Li, Y.L., Meng, J., Cao, K., Wang, P.K., 2012. Dimension of greater India in the early Mesozoic: paleomagnetic constraints from Triassic sediments in the Tethyan Himalaya. J. Asian Earth Sci. 53, 15–24.

Reijmer, J.J.G., 2021. Marine carbonate factories: review and update. Sedimentology 68, 1729–1796.

Riding, R., Liang, L., 2005. Geobiology of microbial carbonates: metazoan and seawater saturation state influences on secular trends during the Phanerozoic. Palaeogeogr. Palaeoclimatol. Palaeoecol. 219, 101–115.

Rigo, M., Preto, N., Roghi, G., Tateo, F., Mietto, P., 2007. A rise in the carbonate compensation depth of western Tethys in the Carnian (Late Triassic): deep-water evidence for the Carnian Pluvial Event. Palaeogeogr. Palaeoclimatol. Palaeoecol. 246, 188–205.

Roghi, G., Gianolla, P., Minarelli, L., Pilati, C., Preto, N., 2010. Palynological correlation of Carnian humid pulses throughout western Tethys. Palaeogeogr. Palaeoclimatol. Palaeoecol. 290, 89–106.

Schlager, W., 1999. Scaling of sedimentation rates and drowning of reefs and carbonate platforms. Geology 27, 183–186.

Schlager, W., 2003. Benthic carbonate factories of the Phanerozoic. Int. J. Earth Sci. 92, 445–464.

Sciunnach, D., Garzanti, E., 2012. Subsidence history of the Tethys Himalaya. Earth Sci. Rev. 111, 179–198.

Scotese, C.R., Schettino, A., 2017. Chapter 3 - Late Permian-early Jurassic Paleogeography of Western Tethys and the World. In: Soto, J.I., Flinch, J.F., Tari, G. (Eds.), Permo-Triassic Salt Provinces of Europe. Elsevier, North Africa and the Atlantic Margins, pp. 57–95.

Seyedmehdi, Z., George, A.D., Tucker, M.E., 2016. Sequence development of a latest Devonian–Tournaisian distally-steepened mixed carbonate–siliciclastic ramp, Canning Basin, Australia. Sediment. Geol. 333, 164–183.

Shi, Z., Preto, N., Jiang, H., Krystyn, L., Zhang, Y., Ogg, J.G., Jin, X., Yuan, J., Yang, X., Du, Y., 2017. Demise of Late Triassic sponge mounds along the northwestern margin of the Yangtze Block, South China: related to the Carnian Pluvial Phase? Palaeogeogr. Palaeoclimatol. Palaeoecol. 474, 247–263.

Sun, Y., Wignall, P., Joachimski, M., Bond, D., Grasby, S., Lai, X., Wang, L., Zhang, Z., Sun, S., 2016. Climate warming, euxinia and carbon isotope perturbations during the Carnian (Triassic) Crisis in South China. Earth Planet. Sci. Lett. 444, 88–100.

Tian, N., Wang, Y., Philippe, M., Li, L., Xie, X., Jiang, Z., 2016. New record of fossil wood Xenoxylon from the Late Triassic in the Sichuan Basin, southern China and its paleoclimatic implications. Palaeogeogr. Palaeoclimatol. Palaeoecol. 464, 65–75.

Tozer, E., 1994. Canadian Triassic ammonoid faunas. In: Bulletin; 467. Geological Survey of Canada, pp. 1–663.

Xia, J., Liao, W., 1986. Some scleractinian corals of procyclolitidae from Lhasa. Acta Palaeontol. Sin. 25, 37-48+125-127.

Yan, Z., Liu, J., Jin, X., Shi, Y., Wang, H., 2019. Construction model and paleogeographic distribution of Late Pennsylvanian phylloid algal - microbial reefs: a case study in eastern. Sediment. Geol. 383, 181–194.

Zhang, S., Li, J., Zhang, H., Wang, L., 2015. Regional Geological Survey of China: Rixin, Zanda and Jiangyema (1:250000). Geology Press, Beijing, pp. 1–224 (in Chinese).

Zhu, R., Yang, Z., Wu, H., Ma, X., Huang, B., Meng, Z., Fang, D., 1998. Paleomagnetic constraints on the tectonic history of the major blocks of China during the Phanerozoic. Sci. China Ser. D Earth Sci. 41, 1–19.